國 立 交 通 大 學

電機與控制工程研究所

碩士論文

以腦波動態變化預估暈車程度

Estimation of Motion Sickness Level based on EEG Dynamics

研 究 生： 魏 群 樹
指導教授： 張 志 永 教授

中 華 民 國 一 百 年 六 月

以腦波動態變化預估暈車程度

Estimation of Motion Sickness Level based on EEG Dynamics

研 究 生：魏群樹　　Student: Chun-Shu Wei

指導教授：張志永 教授　　Advisor: Prof. Jyh-Yeong Chang

國立交通大學

電機與控制工程學系

碩士論文

A Thesis
Submitted to Institute of Electrical and Control Engineering
College of Electrical Engineering
National Chiao Tung University
in Partial Fulfillment of the Requirements
for the Degree of Master
in
Electrical and Control Engineering
June 2011
Hsinchu, Taiwan, Republic of China

中華民國 一百年 六 月

以腦波動態變化預估暈車程度

學生：魏群樹　　指導教授：張志永 博士

國立交通大學電機與控制工程研究所

中文摘要

在日常交通運輸中，最常伴隨的不適症狀即為人們熟知的暈車現象，是一種當大腦接收到衝突的動作感知資訊時所引發的常見症狀。在許多已確認的暈車相關的生理指標中，我們於先前的研究觀察發現以腦電波動態變化預估暈車程度的可行性。相較於傳統的線性迴歸，我們採用輻射基底函數類神經網路(Radial basis function neural network)與支持向量迴歸(Support vector regression)以得到更佳的暈車程度估計。本研究並使用主成分分析和基因特徵選取以提升估計表現至優於過去所用的相關性分析之成效。研究結果顯出使用特徵選取和迴歸方法可有效優化暈車程度之估計，並可引領後續非侵入式暈車監測系統在實際生活之應用發展。

關鍵字：腦電波、獨立成份分析、輻射基底函數類神經網路、支持向量迴歸、主成分分析、基因特徵選取

Estimation of Motion Sickness Level based on EEG Dynamics

Student: Chun-Shu Wei Advisor: Dr. Jyh-Yeong Chang

Institute of Electrical and Control Engineering
National Chiao Tung University

Abstract

Motion sickness is a common symptom that occurs when the brain receives conflicting information about the sensation of movement. Many motion sickness biomarkers have been identified, and electroencephalogram (EEG)-based motion sickness level estimation was found feasible in our previous study. Radial basis function neural network (RBFNN) and support vector regression (SVR) were adopted in this work to approach better motion sickness estimation comparing to the traditional linear regression. This study employs principal component analysis (PCA) and genetic feature selection (GFS) to find usage of EEG features that can further improve estimation performance over the correlation-based method reported in the previous studies. Results of this study demonstrate that these feature selection techniques and regression methods are effective to optimize the estimation of motion-sickness level. This work could lead to a practical system for noninvasive monitoring of the motion sickness of individuals in real-world environments.

Keyword: EEG, Independent Component Analysis (ICA), RBFNN, SVR, PCA, GFS

致　　謝

Acknowledgement

在本論文完成的同時，最須感謝的是的指導教授　張志永教授與　林進燈教授。　張志永教授知人善任，安排我在腦科學研究中心從事有興趣的研究；　林進燈教授提供各種的研究資源以及良好的實驗環境，並常在我研究中迷路時指點方向。感謝兩位老師的助益使我能順利完成論文。

在此衷心感謝美國加州大學聖地牙哥分校的　鍾子平老師以及腦科學中心柯立偉博士在研究上的指導與監督。感謝　鍾子平老師在研究過程中，時常指點迷津，更不吝指導協助學生論文撰寫，讓我於學術能力上獲益匪淺，萬分感恩。感謝柯立偉博士百忙之中仍不厭其煩地與我討論研究，自資料分析至成果展現，皆願意傾囊相授。感謝　鍾子平老師及柯立偉博士一路帶領我學習訊號分析、研究成果發表、乃至做研究的態度，這對我而言是重大的自我改進過程以及一生中難忘的經驗。感謝留下重要研究成果且曾帶領我做專題研究的陳玉潔博士；感謝腦科學中心的邱添丁博士、世安學長、騰毅學長、君玲學姐、冠智學長、倫德學長、尚文學長、俞凱學長、鈞翔學長、奕欣學長、智勝學長、青甫學長、佳玲學姐協助我的研究步上軌道；感謝我的同學：祈翔、旭恩、昱駿、麒宇、幸育；也感謝實驗室的助理們幫忙處理了許多事情。

另外也感謝曾經拉拔我長大的陳右穎教授、欣怡學姐、延泰學長、廷芳學姐、承峰學長、思緯學長、宗城學長、國章學長、宗廷學長、禧岳、怡帆、婉婷，以及曾共患難的夥伴：冠甫、翔宇、修哲、奕奇、勇叡、禹舜。

感謝我的父母兄長，在我困頓失落時作為永遠的靠山，以及純如，一路上陪伴我走過每個辛苦的日子。僅以本文獻給我親愛的朋友、關心我的家人、以及照顧我的師長，願大家能共享我的喜悅與感恩。

Contents

Figures

Tables

1. Introduction

1-1. What Is Motion Sickness

Motion sickness (MS) is a usual response to real, perceived, or even anticipated movement. People tend to get motion sickness on a moving boat, train, airplane, car, or amusement park ride. The most common signs and symptoms of motion sickness include nausea, paleness of the skin, cold sweats, vomiting, dizziness, headache, increased salivation, and fatigue.

1-2. Occurrence of Motion Sickness

The history of MS can be traced back to ancient Greece [1]. Hippocrates, one of the first people to discuss motion sickness, mentioned that motions caused by the ocean disordered the body. Until now, a boat is still the most common environment where motion sickness occurs, because the exposure to motion sickness stimuli is most extensive both with respect to time and motion magnitude during sea travel [2]. The incidence of motion sickness can be as high as 62% on a navy ship [3]. Motion sickness is also often in ground transportation. In a questionnaire survey to identify passengers' personal and environmental factors influencing

individual susceptibility to motion sickness during road transportation, 28.4% of passengers reported feeling ill, 12.8% reported nausea and 1.7% reported vomiting during travel [4]. The malaise of MS may last for more than one hour [5], or even one day [6]. The occurrence of motion sickness is relatively infrequent in an airplane, since modern airplanes are bigger and operate on a higher altitude than previously, and the better weather forecast reduces the chance of encountering with severe weather [1]. In military domain, the increase of simulation training has brought motion sickness problems. After training in a flight simulator, 25% of the air force pilots reported motion sickness symptoms [7].

1-3. Motion Sickness-related EEG

Early studies [8] reported that MS will induce many physiological signal changes including electrogastrography (EGG) [9], galvanic skin responses (GSR) [10], and heart rate variability (HRV) [11]. Recently, the rapid advance in neuroimaging technology has made it able to examine MS-related neural dynamics with EEG, one of the best methods for monitoring the brain dynamics induced by motion-sickness because of its high temporal resolution and portability [8].

Many EEG indicators related motion sickness has been reported in former studies. Delta increase in temporal, frontal, and central area has been found when sickness was induced in

cross-coupled angular stimulation [14], optokinetic rotation drum [9], car-driving VR experiment [16], and object-finding VR experiment [15]. Beta increase in fontal and temporal area was induced in object-finding VR experiment along with motion sickness. Theta increase in frontal, central, temporal, and central area has been reported in experiments of rotating drum [13], parallel swing [12], cross-coupled angular stimulation [14], and optokinetic rotating drum [9]. Nevertheless, theta decrease in central and frontal area was found in the car-driving VR experiment [16].

Apparently, MS-related EEG power changes are not consistent among these cited studies, which may be due to the wide range of paradigms and inconsistent stimulus inputs used to induce motion sickness [8]. Another possible factor making these experiments unreal has been the interruption due to the assessment of the participant's motion sickness level (MSL). Many scholars have adopted a motion-sickness questionnaire by Kennedy et al. [17], a standard rating system for comparing MS states among subjects, to measure susceptibility of subjects to MS. However, it demands interrupting the experiments and asking the subjects to answer few questions. How to provide both visual and vestibular stimulation to induce motion sickness more close to the real life experience? In our past study, Chen et al. performed their experiment on a VR-based driving simulator on a six-degree-freedom motion platform [8]. They also proposed an easy-to-operate online rating mechanism to obtain high temporal resolution self-reporting motion sickness level of individuals.

1-4. EEG Feature Spaces

According to previous review [18], a great variety of features have been employed in EEG-based brain-computer interfaces (BCIs) such as amplitude values of EEG signals [19], band powers [20], power spectral density values [21, 22], autoregressive and adaptive autoregressive parameters [23, 24], time-frequency features [25] and inverse model-based features [26-28]. Among these feature extraction techniques, power spectral density has been considered as one of the most robust and consistent in extracting the distinctive spectral patterns [29]. The spectrum is usually divided into five canonical frequency bands, such as delta (δ: 1–3 Hz), theta (θ: 4–7 Hz), alpha (α: 8–13 Hz), beta (β: 14–30 Hz), and gamma (γ: 31–50 Hz) [30]. In this study, we further separate beta band into low-beta and high-beta bands. Thus, the number of features is six times of the number of electrodes being used. In many such problems, a subset of features will often lead to better dissociation between trial types than the full set of features [31]. However, the number of unique feature subsets for N features is 2^N, a space that cannot be exhaustively explored for N greater than about 25 [31].

1-5. Estimation and Feature Selection in EEG-Based BCI

Typically, the decoding part of BCI involves the technique of classification or estimation, depending on the type of the output, discrete categories or continuous degree. Either classification or estimation, these problems need pattern recognition and machine learning methods to approach highly accurate decoding performance. Since the decoding performance is sensitive to individual deviation and signal noise, the performance of classification is usually more robust than that of estimation in BCI applications. Therefore most EEG-based BCI research aims to decode the brain dynamics into several classes such as emotional states [32] and movement directions [33], but still some studies that focused on estimation problem can achieve high accuracy in single- [34, 35] or cross-subject validation [36].

Prior research has shown the benefits of feature selection in EEG feature space [36]. Among many ways to implement the feature selection search [31, 37, 38], a popular choice is genetic algorithm (GA) [39], which was designed to avoid local optima and has been adopted in EEG feature selection to enhance the performance in BCI applications [33, 40], and GA is also a direct way to extract informative EEG features for experiment amelioration [40].

1-6. Aims of This Study

This study aims to explore the feasibility of building a BCI to continuously estimate the motion sickness level based on the EEG. The structure flow chart is shown as

Figure 1-1.To optimize motion sickness estimation performance, this study involves state-of-art regression methods to improve the estimation model, and applies genetic feature selection to providing better performance through searching ‘good’ feature subsets. In addition, this study also investigates the spatial and temporal dynamics of selected features that support better motion sickness estimation.

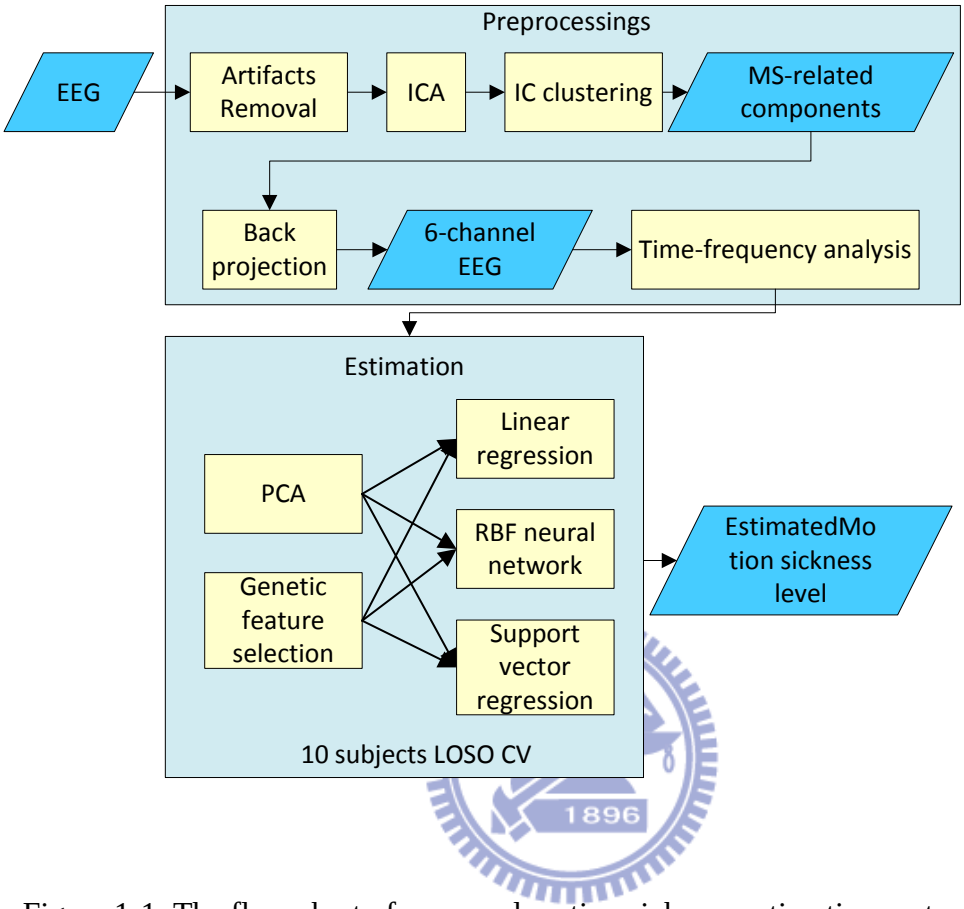

Figure 1-1. The flow chart of proposed motion sickness estimation system.

2. Material and Methods

2-1. Experiment Paradigm of Motion Sickness

Our previous studies [8] have designed and built a 3D virtual-reality (VR) dynamic motion simulator as a test bed for studying (Figure 2-1) driving cognition and motion sickness. The environment provides both visual and vestibular stimuli to participants through the VR environment consisting of 360° projection of VR scenes and a six degree-of-freedom motion platform to induce motion sickness. With such a setup, we expected to induce motion sickness in a manner that is close to what we experience in real life. A three-section experimental protocol was shown as Figure 2-2.

First 10 min is the baseline section involving a straight-road driving. The next 40 min involved driving on a long winding road which often induced subject's motion sickness. Finally, a 15-min recovery section of a straight-road driving was used to help the subjects recover from sickness and back to normal physical status. Eighty percentages of subjects reported motion sickness during the experiments.

Figure 2-1. The immersive VR driving scene with a 360-degree projection.

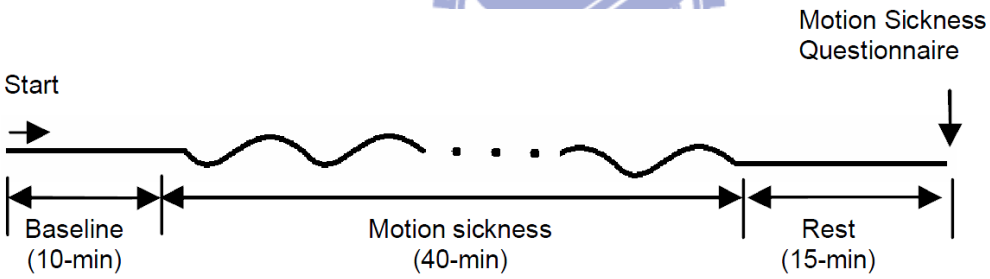

Figure 2-2. Experimental protocol of three-section auto-driving.

2-2. Data Acqusition

2-2-1. Behavior Data Recording

Motion sickness level was continuously reported by the subject who adjusted a joystick with a continuous scale ranging 0 – 5 on its side. The subjects were asked to adjust the scale to a higher level according to their feelings of motion sickness. This continuous MSL was reported in real time without interrupting the experiment rather than the traditional motion-sickness questionnaire (MSQ) proposed in [8].

2-2-2. EEG Recording

The EEG data were recorded from the 10 subjects to examine the brain dynamics during motion sickness. EEG signals were sampled with 500 Hz by a 32-channel NuAmps (BioLink Ltd., Australia).

The acquired EEG signals were first inspected to remove bad EEG channels and then down-sampled to 250 Hz. A high-pass filter with a cut-off frequency at 1 Hz and transition band width 0.2 Hz was used to remove baseline-drifting artifacts and a low-pass filter with a cut-off frequency at 60 Hz and transition band width 7 Hz was used to remove muscular artifacts and line noise. The resultant EEG signals were then fed into the proposed evaluation system for further analysis and the whole process was illustrated by Figure 2-3.

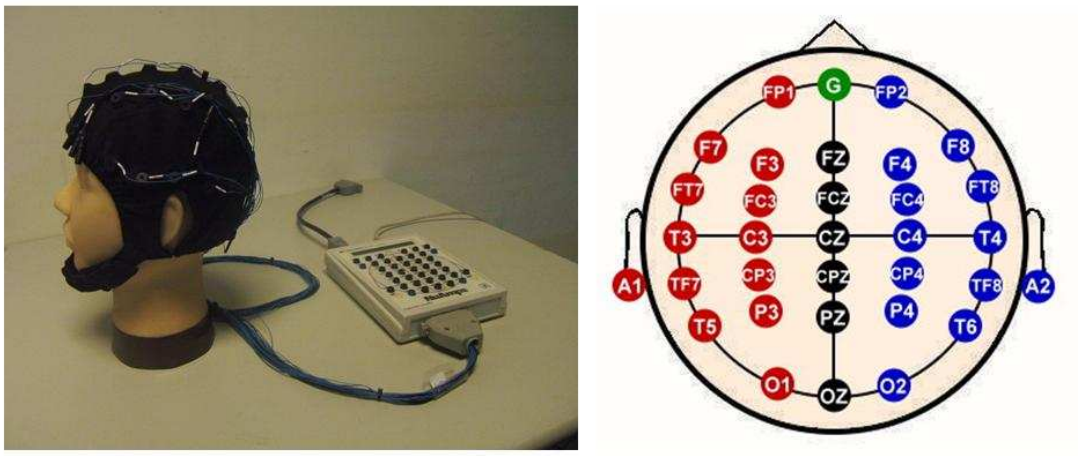

Figure 2-3. The 32 channel EEG cap and electrodes placement of international 10–20 system.

2-3. Independent Component Analysis

Independent Component Analysis (ICA) was applied to EEG recordings to remove various kinds of artifact, such as blink artifact and indoor power-line noise, and to extract features of human's cognitive task. Independent component analysis is a novel statistical technique to find out the linear projections of the data that can maximize the mutual independences of estimated components, and has been proven as an effective technique to solve blind source separation (BSS) problem. Therefore, ICA decomposition is a usefully computational method for EEG signal processing. It can separate an observed multivariate

signal into several cumulative segments under the assumption of the mutual statistical independence of the non-Gaussian source signals. The general representation of ICA model can be simply denoted as $S = W \times X$, where $S = [S_1, S_2, S_3, ..., S_n]^T$ presents the n independent sources, W is the weighting matrix, and $X = [X_1, X_2, X_3, ..., X_n]^T$ is the n observed signals. The purpose of ICA algorithm is to find out a weighting matrix, W, to have a maximum statistically independency of the separated components.

2-4. Component Clustering

After doing ICA process, component clustering was analyzed using DIPFIT2 routines [41], a plug-in in EEGLAB [42], to find the 3D location of an equivalent dipole or dipoles based on a four-shell spherical head model. Among components from all subjects, those with similar scalp topographies, dipole locations and power spectra were clustered. Ten component clusters recruited more than 10 components from multiple subjects with similar topographic maps were regarded as robust component clusters. Figure 2-4 showed the five most MSL-related clusters were selected in our previous study [8]. The component usage sorted by subject was shown in Table 2-1. According to Table 2-1, we can find that not all subjects have every motion sickness related components because the level of motion sickness induced by vestibular and visual stimuli to each subject had the significant individual difference.

According to MSQ results and subject's self-response of motion sickness, we can confirm that each subject indeed felt sickness during the whole experiment session. Consequently, these extracted components are correlated with motion sickness. Then we can feed the ICA signals into the evaluation system for next step, back projection.

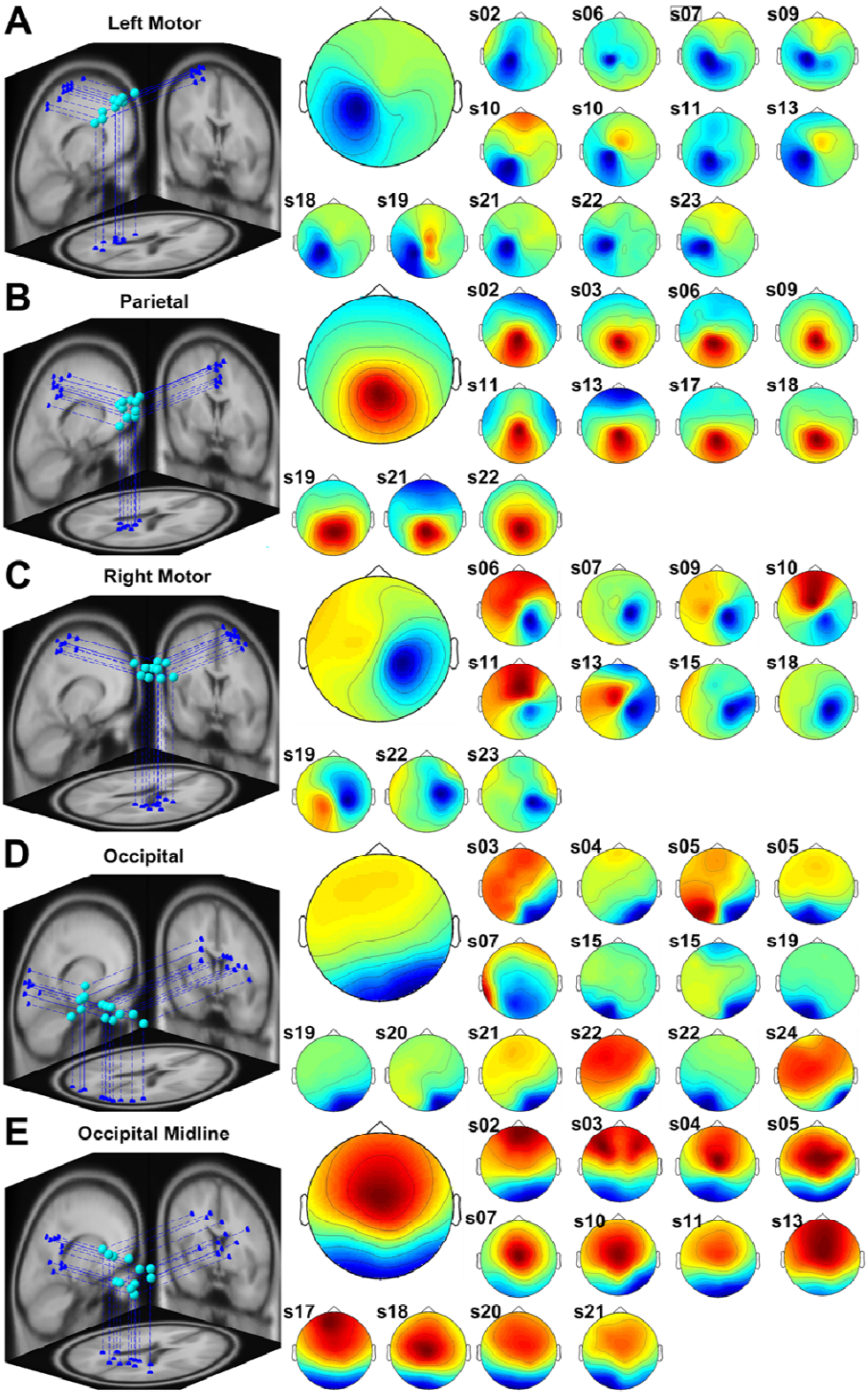

Figure 2-4. Five component clusters highly correlated with motion sickness in our previous study [8].

Table 2-1. Component separation of each subject.

Subject	Left motor	Parietal	Right motor	Occipital	Occipital Midline
S1	●	●			●
S2				●	●
S3	●		●	●	●
S4	●●		●		
S5	●	●	●		●
S6			●	●●	
S7	●	●	●		●
S8				●	●
S9	●	●		●	●
S10	●		●		

●: One selected component; ●●: Two selected components.

2-5. Component Activities Back Projected to Channel Activities

As previously mentioned, the extracted independent components are different in number and in location through subjects. To maintain the consistency of subject data, we proposed to project these components back on channel domain. The channels of interest (Fp1, Fp2, C3, C4, Pz, and Oz) in this study are those electrodes close to the MS-related component clusters stated in our previous study [8]. C3 and C4 are close to left and right motor region respectively. Pz and Oz mostly represent the activity of parietal, occipital, and occipital midline areas. Frontal electrodes (Fp1 and Fp2) are relatively distant from the MS-related component clusters, but they are included in the channels of interest. The reason is that forehead, which is not covered by hair, is a popular choice to place EEG sensors, and the state-of-art EEG-based BCI devices using dry sensor on forehead have been developed in recent years [43, 44].

2-6. Time-Frequency Analysis

Time-frequency analysis was applied to investigate the component dynamics in frequency domain. The spectra of the components from 1 Hz to 50 Hz were calculated using 180-second window with 150-second overlap, and subdivided into several 250-point

sub-windows with 125-point overlaps. Each window was zero-padded to 256 points for using 256-point fast Fourier transform (FFT) with ~1 Hz resolution in frequency. The 180-second window length is determined according to our previous study [35], where the estimation performance was improved by a 3-min smoothing window. The process of time-frequency analysis is illustrated in Figure 2-5. The time-frequency spectral power was then converted into decibel power, and the power during winding road section was further extracted and normalized using Z-score approach. The normalized spectral powers of 6 bands from 6 channels, totally 36 features, were used as the input predictors in MSL estimation.

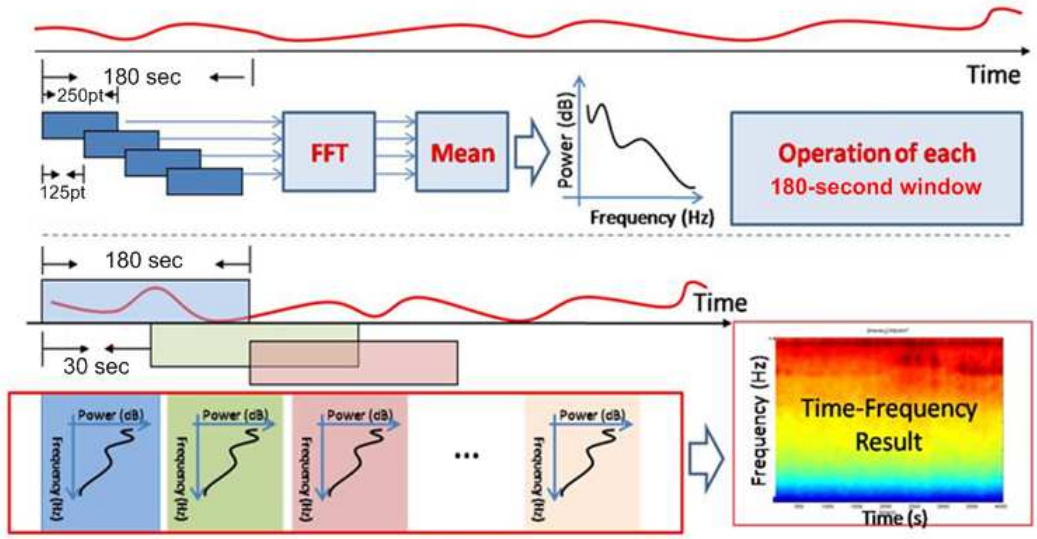

Figure 2-5. Time-frequency analysis procedure used to obtain dynamic EEG frequency responses during the experiments.

2-7. Motion Sickness Level Estimation

This study investigates the feasibility of an EEG-based motion-sickness evaluation system, and compares the MSL estimation performance obtained by three different regression methods: 1) linear regression (LR), 2) radial basis function neural network (RBFNN), and 3)

support vector regression (SVR). Results of MSL estimation demonstrate the practical potential of accurate and continuous motion-sickness estimation based on non-invasive EEG.

2-7-1. Radial Basis Function Neural Network

Radial basis function neural network (RBFNN) is a feed-forward structure network consisting of three layers: input layer, one single hidden layer with a nonlinear activation function, and a linear output layer (Figure 2-6) [45].

The output y_{out} is defined as

$$y_{out} = \varphi(x) = \sum_{k=1}^{M} w_k \cdot A(x_k, c_k, \sigma_k) \quad (1)$$

The activation function *A* is Gaussian radial basis function:

$$A(x, c, \sigma) = e^{-\|x-c\|^2 / 2\sigma^2} \quad (2)$$

where w_k is linear combinational weight, c_k is the centers of Gaussian radial basis function with variance σ_k. The error cost function is:

$$E(t) = (\sum_{k=1}^{M} w_k(t) \cdot A(x_k, c_k, \sigma_k) - y(t))^2 \quad (3)$$

which is minimized with orthogonal least-square and gradient descent learning algorithm.

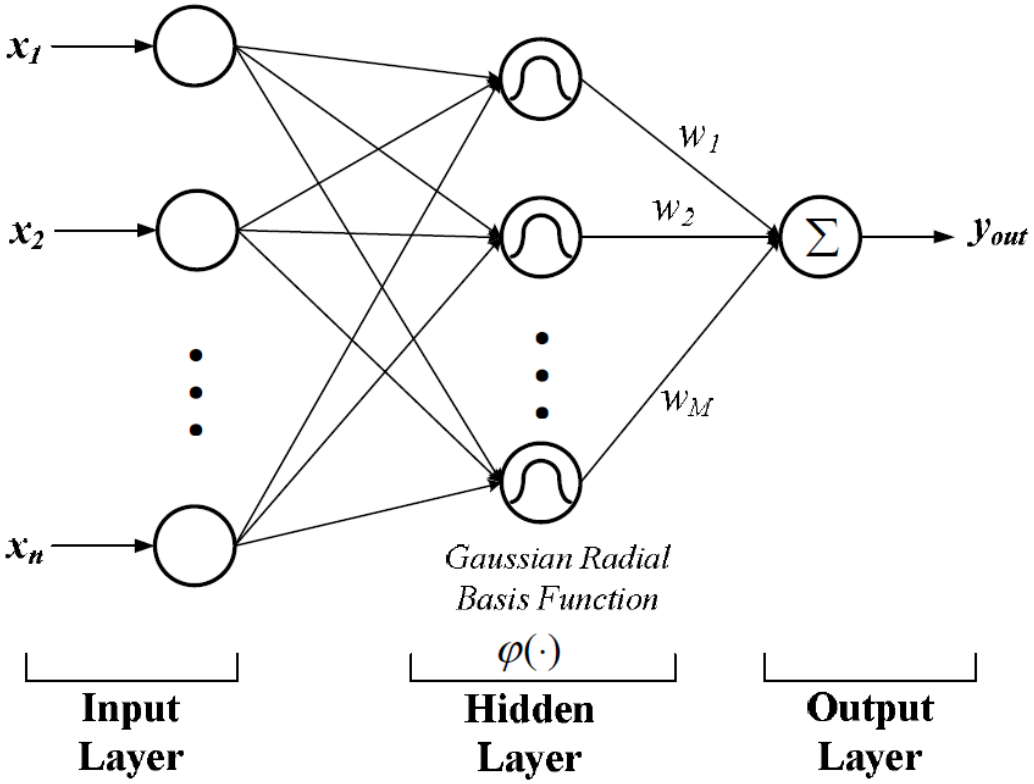

Figure 2-6. Structure of RBF Neural Network.

2-7-2. Support Vector Regression

Support vector machine (SVM) is a novel tool commonly applied for classification and regression by nonlinearly mapping labeled dataset to a higher dimensional feature space. In particular, ε-support vector regression (SVR) has been developed for solving regression

problems [46]. Given a training data set $\{x_i\}_{i=1}^N$ and output data set $\{y_i\}_{i=1}^N$, the problem is to minimize:

$$\frac{1}{2}\|w\|^2 + C\left(\sum_{i=1}^{N}(\zeta_i + \zeta_i^*)\right)$$

subject to $\begin{cases} y_i - f_i \le \varepsilon + \zeta_i^* \\ f_i - y_i \le \varepsilon + \zeta_i \end{cases}$, $\zeta_i^*, \zeta_i \ge 0$

where C is a user-defined constant which was 1 is this work. The mapping function is:

$$f(x) = \sum_{i=1}^{N}(a_i - a_i^*)\kappa(x_i, x) + b \tag{4}$$

where the kernel function κ is:

$$\kappa(x_i, x_j) = \left(\phi(x_i) \cdot \phi(x_j)\right) \tag{5}$$

Here we adopted Gaussian radial basis function kernel:

$$\kappa(x, y) = e^{-\|x-y\|^2/2\sigma^2} \tag{6}$$

2-8. Genetic Feature Selection

The selection problem in this study means searching a best feature subset from all 250 possible combinations. A popular choice is genetic algorithm (GA) [39], which was designed to avoid local optima and has been adopted in EEG feature selection to enhance the performance in BCI applications [33, 40]. In this study, each chromosome of the population is assigned with a 50-bit sequence as the selection is among all 50 features, where 1 indicates the feature was selected and 0 indicates it was not selected. Here the genetic feature selection (GFS) was implemented under Matlab environment using stochastic uniform member selection and scattered crossover. Each bit in each chromosome is flipped with mutation rate 0.01 to produce new selections. The fitness of a chromosome is defined as to the performance of estimation, which was the modified Akaike information criterion (AIC) [47] including correlation coefficient (CC), mean square error (MSE), and a penalty for large dimension size:

$$AIC = W_f N_f + W_e \ln(MSE) + W_c \ln(1 - CC^2) \quad (7)$$

where N_f is the number of selected features and W_f, W_e, and W_c are positive weights (0.01, 0.1, and 1) given according to the importance of each term. The feature selection system architecture is shown in Figure 2-7. The process involved 50 generations of 5-fold cross validation training by estimator with 20 individuals, and the performance of each individual was assessed by the CC and MSE between the actual MSL response and the estimated response obtained using estimator.

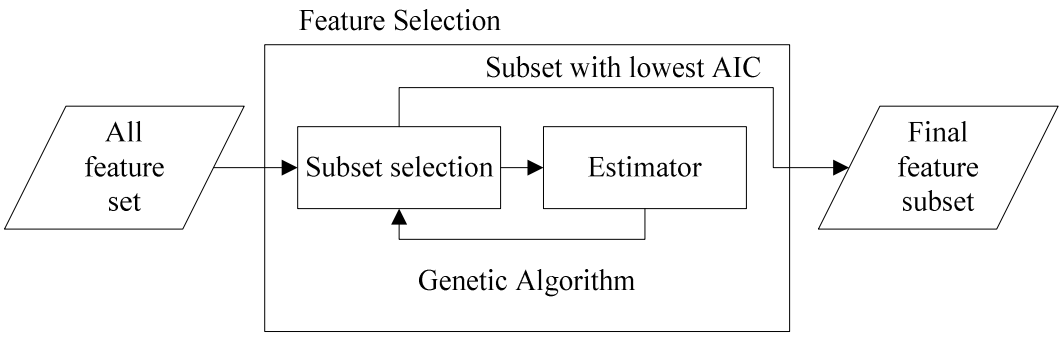

Figure 2-7. The process of genetic feature selection.

2-9. Principal Component Analysis

When using EEG spectral power as features, one feature tends to have similar fluctuations with those at its neighboring frequencies, and it could be redundant to include features with adjacent frequencies [36]. A simple and popular solution is to apply principal component analysis (PCA), which has been widely used as a tool to reduce the data dimension and to extract eigenvectors in EEG-based BCI applications [35, 48, 49].

The goal of PCA [50] is to find a set of $p < d$ vectors in $\Re^d$ space explaining the maximum amount of variance in the data. Suppose that the data has been centered in the original space and v is an arbitrary normalized vector in $\Re^d$. The first eigenvector can be found by

$$v = \underset{v \in \Re^d, \| v \| = 1}{\arg\max} \; v^T C v \tag{8}$$

where v is the $d \times d$ covariance matrix. The solution of the above equation is the eigenvector v of C with respect to the largest eigenvalue. One can seek the direction of the second eigenvector by looking for the second largest variance, and so on. Traditionally, the eigenvector is selected according to the order of eigenvalue from the largest to the smallest,

and the number of selected eigenvectors is a parameter which can be determined in training process.

In this study, the number of selected eigenvector was determined in the PCA training process (Figure 2-8). Leave-one-subject-out (LOSO) cross validation was performed to evaluate the estimation performance. In LOSO cross validation, each subject's data was prepared as the testing data, and the data from the other 9 subjects were collected as the training data. PCA was performed on the training data to extract the eigenvectors for selection and projection. And then in the training data, another LOSO cross validation was performed repeatedly using from 1 to all 36 eigenvectors. Finally, the number of eigenvectors that support the least average AIC across 9 training subjects in the training process was used in the testing process.

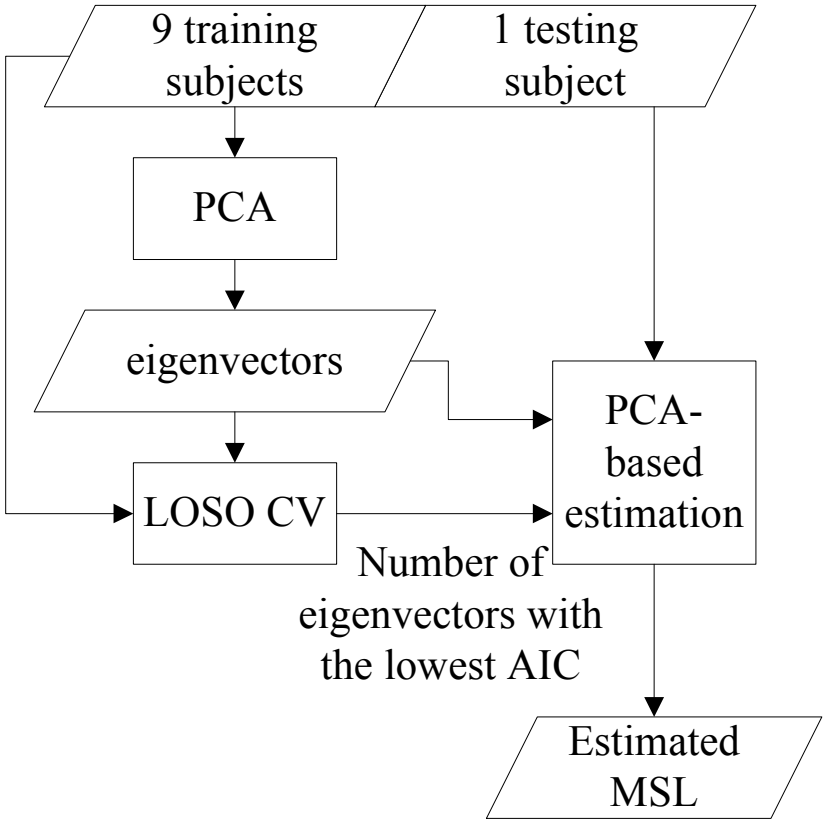

Figure 2-8. The training process of PCA-based methods.

3. Experimental Results

3-1. Comparison between Regression Methods

The results of this study were processed by multiple comparison tests. Three-way analysis of variance (ANOVA) and Wilcoxon signed-rank test to examine whether the

difference is significant or not for the three factors: subjects, regression methods (LR, RBFNN, and SVR), and feature selection techniques (All-feature, PCA, GFS). After ANOVA, sign-rank test was performed to estimate the p-value for testing the significance of difference between pairs of techniques. The statistical results will be discussed in detail in the next chapter.

In Figure 3-1, all of the estimation techniques consisting of different regression and feature selection methods were compare together in aspects of correlation coefficient (CC) and root-mean-square-error (RMSE) between the estimated and the actual MSL response. RBFNN and SVR both outperformed LR significantly in CC and RMSE under all-feature condition, increasing the average CC by 0.1385 and 0.1237 respectively, and reducing the average RMSE by 0.0743 and 0.0613 respectively. Most techniques showed significant difference from LR in estimation performance, except in the case using PCA+RBFNN was not significantly different in RMSE, and GFS+LR was not in both CC and RMSE ($p > 0.05$).

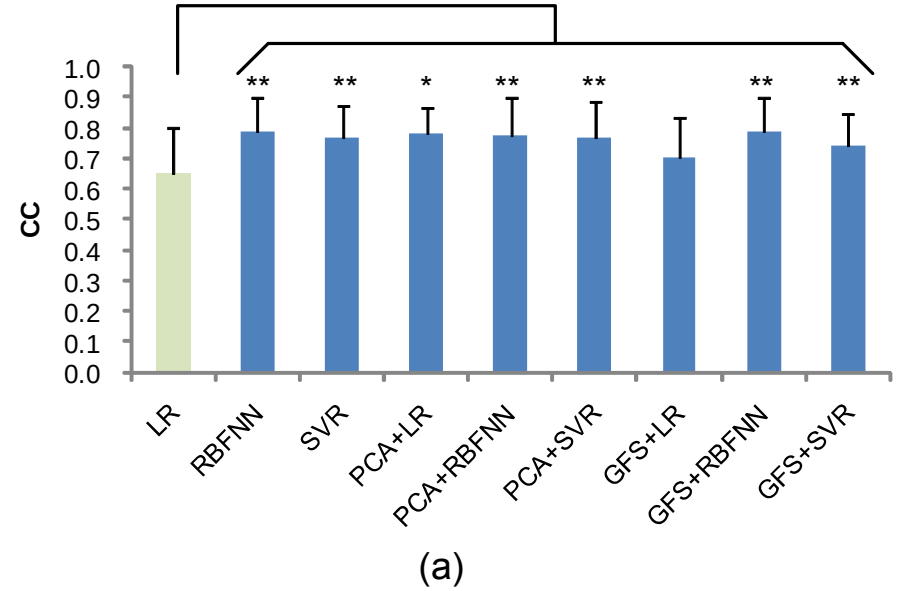

Figure 3-1. Comparison of the feature selection and regression techniques' performance of (a) CC and (b) RMSE averaged over 10 subjects. Vertical lines denote the intersubject standard deviations of the respective mean CC and RMSE values. Wilcoxon signed-rank test was performed to evaluate the significant difference between LR and each other technique (*$p < 0.05$, **$p < 0.01$).

3-2. Comparison between Feature Selection Methods

Figure 3-2 shows the number of eigenvectors used in PCA-based methods and the number of features selected in GFS-based methods. In Figure 3-2(a), the ability of PCA in dimension reduction was revealed by the small number of eigenvectors used by three techniques. In comparison, different regression methods show different demand for eigenvectors. Both RBFNN and SVR tend to adopt less eigenvectors than LR and show significant difference in the number of eigenvectors ($p < 0.05$), and the number is especially small in RBFNN ($p < 0.01$). In Figure 3-2(b), the number of feature selected by GFS-based methods are reduced, showing GFS also provide the benefit in dimension reduction. In the comparison of number of features selected in the three techniques, GFS+SVR tends to selected more features than GFS+LR ($p < 0.05$), while GFS+RBFNN has no significant difference in number of features with GFS+LR ($p > 0.05$).

The examples of the estimated MSL during the winding road section in the experiment from two subjects, S1 and S8, are presented in (a) and (b) respectively. In both plots the estimated MSL show the same ascendant tendency as the actual MSL does, but a difference is that the estimated MSL rise ahead of the actual MSL in these two cases. The best performances of subjects are summarized in Table 3-1.

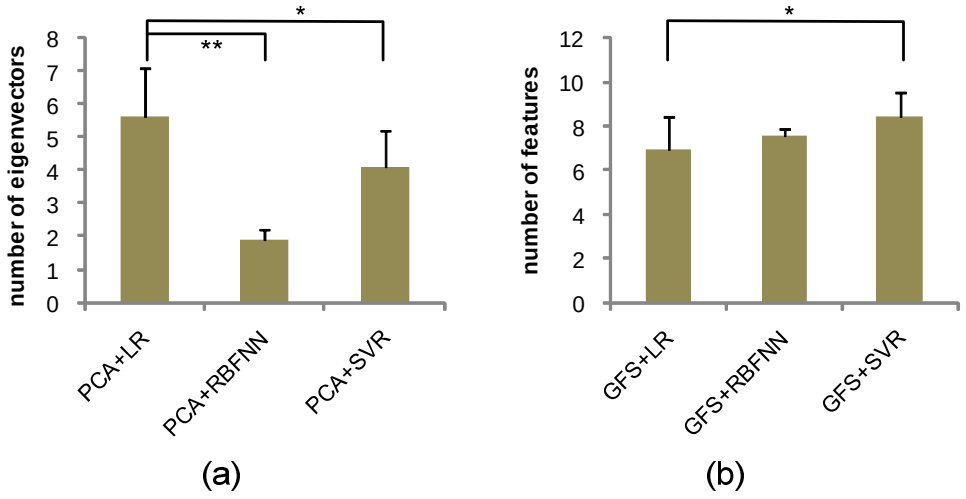

Figure 3-2. Comparison of number of (a) eigenvectors and (b) features correspondent to the regression methods averaged over 10 subjects. Vertical lines denote the intersubject standard deviations of the respective mean eigenvector and feature values. Wilcoxon signed-rank test was performed to evaluate the significant difference between LR and each other technique (*$p < 0.05$, **$p < 0.01$).

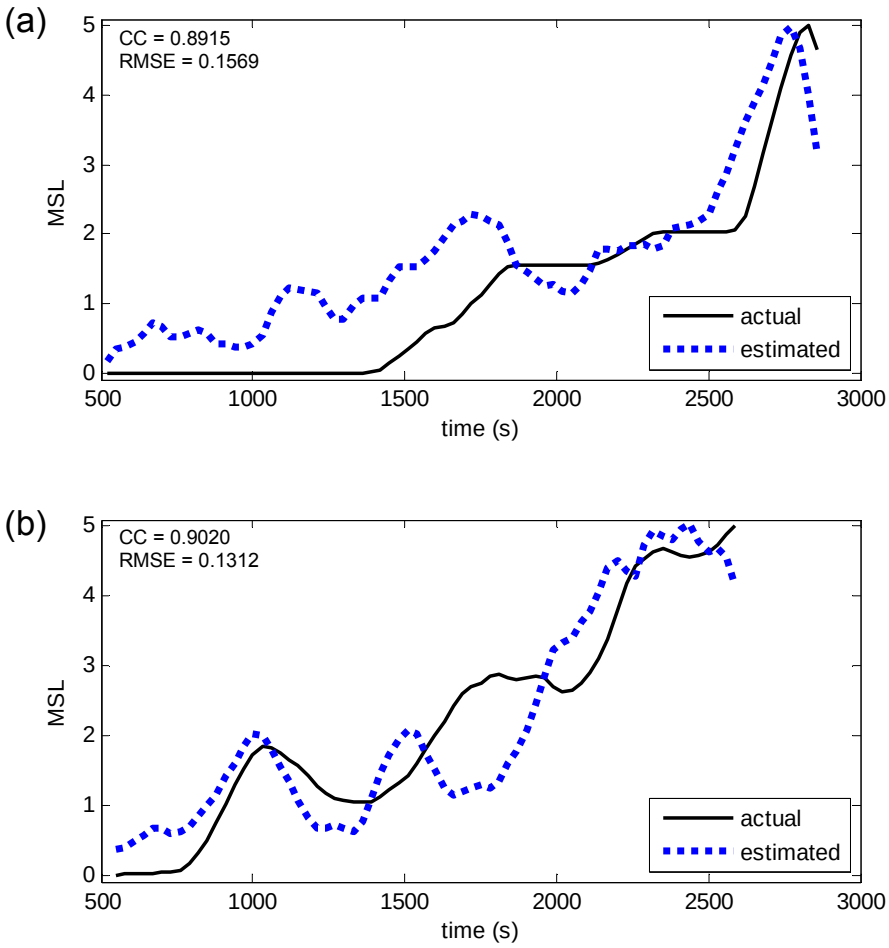

Figure 3- 3. Estimation results of (a) S1 using PCA+SVR, and (b) S8 using GFS+SVR. Black thick line is the actual MSL response during winding road section, and blue dotted line is the estimated MSL response.

Table 3-1. The best performance and technique of each subject.

Subject	CC	Technique	RMSE	Technique
1	0.9008	GFS+RNN	0.1569	PCA+SVR
2	0.8638	GFS+SVR	0.1843	SVR
3	0.8503	SVR	0.1502	RNN
4	0.9198	GFS+RNN	0.1987	PCA+SVR
5	0.6605	PCA+LR	0.3327	PCA+LR
6	0.7494	PCA+LR	0.2302	PCA+LR
7	0.8804	GFS+RNN	0.2390	PCA+SVR
8	0.9036	GFS+SVR	0.1312	GFS+SVR
9	0.9220	GFS+SVR	0.1334	GFS+SVR
10	0.6892	GFS+RNN	0.2365	RNN
Average	0.8340		0.1993	
SD	0.0977		0.0625	

3-3. The Eigenvectors in Principal Component Analysis

Figure 3-4 shows the eigenvectors extracted in the training process for a single subject. The uniformity of all feature weights in first eigenvector reveals that the most principal component of the training data is the summation of all features. The second eigenvector has positive weights in lower frequency bands and negative weights in higher frequency bands, which means that the second principal component is the difference between lower and higher

frequency band powers. Likewise, the third principal component is the difference between delta- and theta- power, and so on.

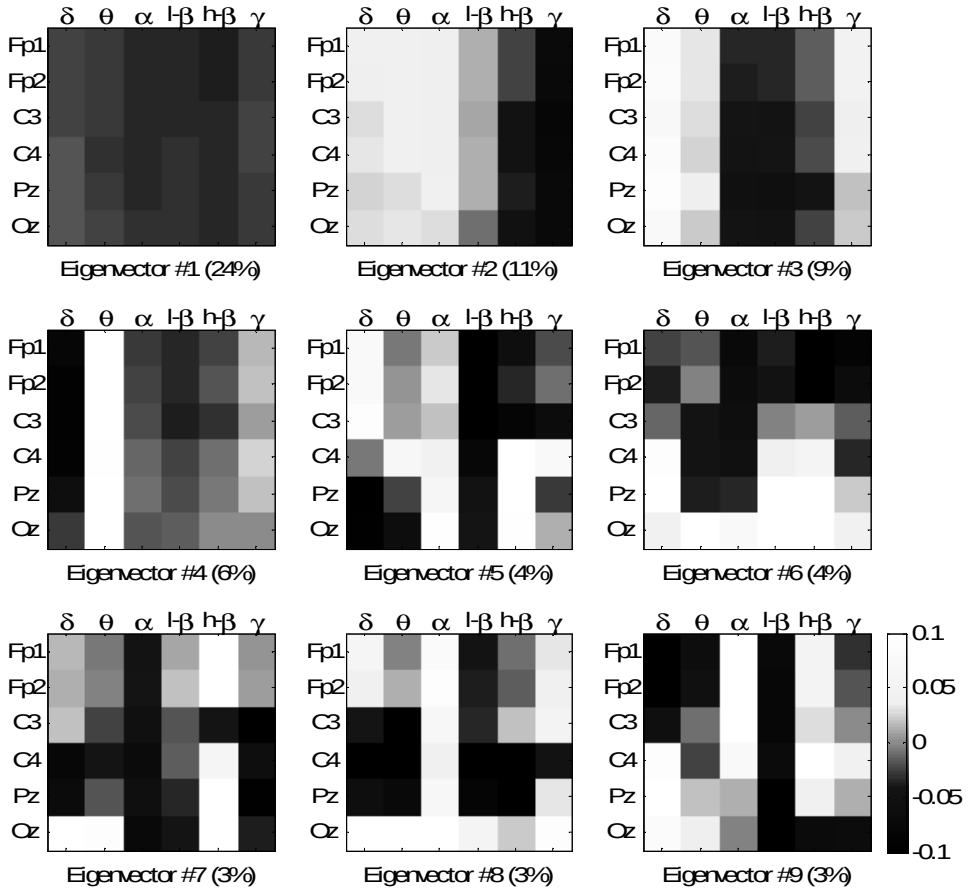

Figure 3-4. The weights of eigenvectors extracted in the training process for S1. The first 9 of 36 eigenvectors ranked by the value of eigenvalue are shown here with the ratios of eigenvalue. In our experimental result, the first 7 eigenvectors were used for PCA+LR, 2 for PCA+RNN, and 5 for PCA+SVR. Bright pixels represent positive feature weights, and dark pixels represent negative feature weights.

3-4. Fitness Evolution in Genetic Feature Selection

The evolution in GFS improved the fitness of the population every new generation, and the monotonic descend of AIC is illustrated in Figure 3-5(a). This sample process approached its best fitness within 20 generations and then optimized the whole population. The CC and RMSE performances in the evolution process are shown in Figure 3-5(b) and (c) respectively. As illustrated in Figure 3-5(b) and (c), the CC and RMSE performances obtained in the end of the evolution were not the best during the process of evolution. This phenomenon will be discussed in detail in the next chapter.

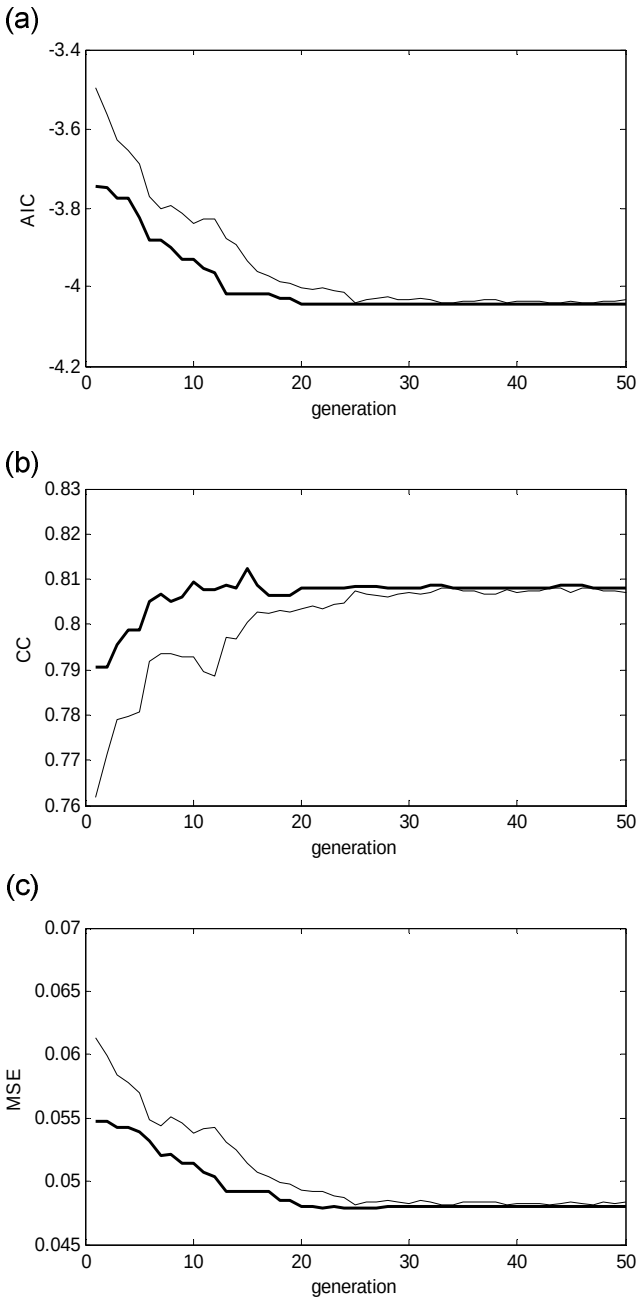

Figure 3-5. An evolution example of (a) Akaike information criterion (AIC), (b) correlation coefficient (CC), and (c) root-mean-square-error (RMSE) over generations in genetic feature selection (GFS). Thick line stands for the best fitness, and the thin line is for the average fitness.

3-5. The Selection Results of Genetic Feature Selection

The results of feature selection by GFS-based methods are presented in Figure 3-6 with feature selection probability averaged across all subjects. The features with high selection probability are shown as bright pixels, and dark pixels represent those with low selection probability. Table 3-2 lists the top 6 frequently-selected features among all 36 features in these GFS-based methods. Three of these features are listed in the top 6 across all three GFS-based methods: alpha in Fp1, alpha in Oz, and high beta in Oz.

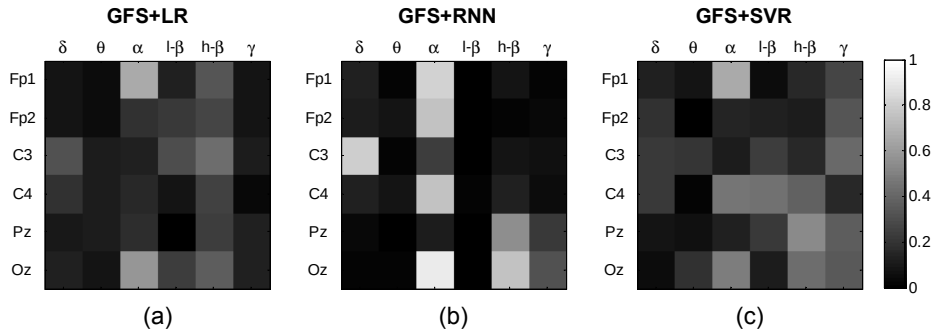

Figure 3-6. Average feature selection probability for the three regression methods combined with genetic feature selection. (a) GFS+LR, (b) GFS+RNN, and (c) GFS+SVR across 10 subjects.

Table 3-2. The top 6 popular feature selected in each GFS-based method.

GFS+LR			GFS+RBFNN			GFS+SVR		
channel	band	probability	channel	band	probability	channel	band	probability
Fp1	α	0.67	Oz	α	0.92	Fp1	α	0.66
Oz	α	0.59	Fp1	α	0.82	Pz	h-β	0.54
C3	h-β	0.43	Oz	h-β	0.76	Oz	α	0.49
Oz	h-β	0.36	Fp2	α	0.76	C4	α	0.46
Fp1	h-β	0.34	C4	α	0.75	C4	l-β	0.44
C3	δ	0.32	Pz	h-β	0.56	Oz	h-β	0.43

4. Discussion

4-1. Factors Affecting Estimation Performance

The three-way ANOVA was performed to verify if difference is significant for the factors (subjects, regression methods, and feature selection techniques). All of the three factors were found to significantly affect the performance in CC ($p < 0.05$), but only two factors (subjects and regression methods) were found to significantly affect the performance in RMSE ($p < 0.05$). The factor of feature selection techniques did not show significance in affecting the RMSE performance. Comparing the affection to estimation performance

produced by regression methods and feature selection techniques, the former seems to be more deterministic since it significantly impacts performance in both CC and RMSE.

4-2. Comparison between Regression Methods

In this study, linear regression was employed as a baseline regression method and to be compared with other two methods, RBFNN and SVR. The result shows that both RBFNN and SVR provide better estimation performance with different types of feature selection in our case. In comparison of RBFNN and SVR, the later shows significant difference with LR no matter using all-feature, PCA, or GFS, while RBFNN fail to reduce RMSE significantly when combining with PCA. However, RBFNN shows its unique characteristics in the usage of features and eigenvectors. The number of eigenvector selected by RBFNN is significantly less than selected by other methods, implicating RBFNN works well with low-redundancy data.

SVM has been reported as a optimal classifier in EEG-based BCI [18],[29]. Although regression is not as commonly induced as classification in EEG-based BCI application, SVR has been shown its benefit in optimizing the EEG-based 2-dimentional movement control [51]. In our case, SVR enhanced the estimation performance in each combination of feature selection type, and thus it is suggested as a useful regression method to improve the performance.

4-3. Comparison between Feature Selection Methods

PCA and GFS are induced in this study to provide information about what kind of the use of features optimizes the estimation result. Through PCA, the use of features is determined by the selection of eigenvectors and the feature weights in each eigenvector. While all features are involved in PCA to extract these eigenvectors, GFS gives a direct view by counting the selected times of each feature and shows which features are more popular in MSL estimation. Overall, these two feature selection techniques did not support better estimation performance when combining with RBFNN and SVR. However, adding PCA in LR significantly enhanced the estimation performance to be comparable with RBFNN and SVR in MSL estimation.

4-4. Difficulty caused by Subject Variation

It has been shown the subject deviation significantly affects the estimation performance in this study. Subject-to-subject variation has been regarded as one of the major source of error [18], and it is the most dominant factor in MSL estimation. In our previous work on MSL estimation using within-subject validation, the performance in CC could reach 0.95

without optimization of genetic algorithm, which obviously exceeds the performance using cross-subject validation in this work where the best CC performance is around 0.92. However, it is necessary for an EEG-based BCI application to test its performance in cross-subject validation, which provides general examination and is more beneficial for future implementation or other practical applications.

4-5. The Benefit of Principal Component Analysis

Our result shows the linear regression was improved significantly when using PCA in prior. In fact, this combination is a typical regression analysis as known as 'principal component regression (PCR)' [52]. Instead of using the variables to estimate the regression coefficients, PCR estimates with the principal component of those variables. EEG spectral power, although being regarded comparatively as a robust feature type, has been reported its redundancy caused by the correlation between frequencies [36]. A practical benefit of using PCR is its ability to overcome the problems caused by the co-linearity between variables, and thus PCR is a simple and useful tool to enhance the estimation performance of BCI applications based on EEG spectral power.

Instead of the purpose of improving the estimation performance, PCA was employed as tool to probe the property of the data. In our case, the most principal component is the

summation of all features, and there is only apparent difference between frequency bands but no deviation between channels are revealed from the feature weights in the first four eigenvectors. While through the estimation technique PCA+RBFNN can reach rather high performance with about using only two eigenvectors, this suggests the obvious redundancy in our data, and again, evidence the benefit of using PCA.

4-6. The Benefit of Genetic Feature Selection

In the evolution process of GFS shown in Figure 3-5, the AIC descended monotonically as expected. Meanwhile, CC and RMSE reached their best during the process of evolution but did not persist until the end. Consider that the modified AIC applied in this study was a combination of CC performance, RMSE performance, and dimensional penalty; it is obvious to see that the fitness was dependant on every measure. Therefore, the trade-off process was involved in the evolution, and the final outcome was a consequence of compromise.

Although genetic algorithm is well-known for its ability to avoid local optima, the time-consuming evolution process forced us to limit the population size and generations in our implementation, and thus our compromise suppressed the average performance of 10 repeated runs of GFS-based methods. But still the best performances in most subjects were obtained by GFS-based methods. While the estimation performance was obviously improved

by using RBFNN and SVR, the effects of PCA and GFS were not so apparent on optimizing the regression methods. However, the benefit of feature selection was not only improving the estimation performance, but also providing informative feature selection result as an approach to understand the property of the data used. In the feature selection results presented in Figure 3-6 and Table 3-2, the features most popularly selected across different techniques are alpha in Fp1, alpha in Oz, and high-beta in Oz.

In our previous study using ICA to extract MS-related component, the brain activity in occipital midline was the most emphasized component which showed significant power difference between low and high MSL conditions across broad frequency band [8]. In the same study, the secondary MS-related component was occipital, which has particular significant power difference in alpha band reflecting change in MSL. As mentioned previously, Oz was chosen and expected to represent the brain dynamics in occipital area. Therefore, the high selection probability of alpha in Oz meets our anticipation that it is important in MSL estimation since it was integrated mostly from the significant MS-related components according to the previous findings.

High-beta band power, although was not emphasized, its relation with motion sickness was still revealed in the correlation analysis performed in our previous study [8]. The correlation around 20 to 25 Hz was shown higher than other frequency bands except of alpha band in occipital and occipital midline component.

Another finding in the feature selection is that alpha in Fp1 was almost as frequently chosen as alpha in Oz. Although few researchers have reported EEG increase in frontal area during motion sickness [12, 14-16], we did not find MS-related component in frontal using ICA and source localization. Since the Fp1 and Fp2 activity used in this study was extracted from back projection using MS-related component in motor, parietal, and occipital areas, it is not comparable with the frontal activity directly recorded by frontal electrodes in other studies. For an electrode placed on frontal, it is difficult to sense the brain activity in parietal and occipital since the distance attenuates the amplitude of signal, and augments the noise. However, the result in this study shows that alpha in Fp1 may play an important role in MSL estimation. If the technique of noise filtering or source separation is powerful enough to allow frontal electrodes to detect the activities from the whole brain, one will consider using frontal electrodes to collect EEGs for motion sickness estimation. The reason is that it is easier to fit EEG electrodes on forehead because there is no hair on it. Recently, the state-of-art wearable and wireless EEG-based BCI devices using dry-electrode on forehead have been developed and demonstrated [43, 44].

5. Conclusion and Future Works

This study showed that changes in the EEG spectral power accompany fluctuations in the level of motion sickness, as assessed by measuring simultaneous changes in EEG and self-reported motion-sickness level in a VR-based driving task. We demonstrated the potential of a BCI for continuously estimating motion sickness based on EEG spectra, compared the usability of feature selection techniques combining with different regression algorithms. Results of MS estimation using the EEG features selected by principal component analysis and genetic feature selection compare favorably to previous results using a correlation-based method [35], but in this study the feature's contribution to estimation is more emphasized.

The work is the first step towards developing a BCI that can continuously monitor the pre-cursor of motion sickness. If one could accurately predict motion sickness before its occurrence, it would be possible to apply certain treatments to prevent illness instead of taking pills nowadays. The ultimate goal of our study is to help people avoid motion sickness and thus prevent individual's illness and derived danger caused by motion sickness.

References

[1] J. Dahlman, “Psychophysiological and Performance Aspects on Motion Sickness,” *University dissertation from Linköping*, vol. 1071.

[2] J. Reason and J. J. Brand, *Motion sickness*, Academic Press, 1975.

[3] A. Rolnick, “Seasickness incidence in the Israeli Navy,” in *Israel Navy report C- 101: Tel Aviv*, Israel, 1985.

[4] M. Turner and M. J. Griffin, “Motion sickness in public road transport: the effect of driver, route and vehicle,” *Ergonomics*, vol. 42, no. 12, p. 1646, 1999.

[5] R. S. Kellogg, C. Castore, and R. Coward, “Psychological effects of training in a full vision simulator,” *Annual Scientific Meeting of the Aerospace Medical Association*, 1980.

[6] J. Gower, W. Daniel, and J. Fowlkes, “Simulator Sickness in the UH-60 (Black Hawk) Flight Simulator,” *U. S. Army Aeromedical Research Laboratory*, 1989.

[7] E. R. Muth and B. Lawson, “Using flight simulators aboard ships: human side effects of an optimal scenario with smooth seas,” *Aviation, Space, and Environmental Medicine*, vol. 74, no. 5, pp. 497-505, May. 2003.

[8] Y.-C. Chen, J.-R. Duann, S.-W. Chuang, C.-L. Lin, L.-W. Ko, T.-P. Jung, and C.-T. Lin, “Spatial and temporal EEG dynamics of motion sickness,” *NeuroImage*, vol. 49, no. 3, pp. 2862-2870, Feb. 2010.

[9] S. Hu, W. F. Grant, R. M. Stern, and K. L. Koch, “Motion sickness severity and physiological correlates during repeated exposures to a rotating optokinetic drum,” *Aviation, Space, and Environmental Medicine*, vol. 62, no. 4, pp. 308-314, Apr. 1991.

[10] B. Cheung and P. Vaitkus, “Perspectives of electrogastrography and motion sickness,” *Brain Research Bulletin*, vol. 47, no. 5, pp. 421-431, Nov. 1998.

[11] S. R. Holmes and M. J. Griffin, “Correlation Between Heart Rate and the Severity of Motion SicknessCaused by Optokinetic Stimulation,” *Journal of Psychophysiology*, vol. 15, no. 1, pp. 35-42, 2001.

[12] J. P. Wu, “EEG Changes in Man During Motion-Sickness Induced by Parallel Swing,” *Space Med. Med. Eng.*, vol. 5, no. 3, pp. 200 - 205.

[13] J. J. Wood, F. A. Struve, J. J. Straumanis, J. J. Stewart, and C. D. Wood, “The effect of motion sickness on brain waves (EEG),” *Aviat Space Environ Med.*, vol. 62, no. 461, 1991.

[14] W. E. Chelen, M. Kabrisky, and S. K. Rogers, “Spectral analysis of the electroencephalographic response to motion sickness,” *Aviation, Space, and Environmental Medicine*, vol. 64, no. 1, pp. 24-29, Jan. 1993.

[15] Y. Y. Kim, H. J. Kim, E. N. Kim, H. D. Ko, and H. T. Kim, “Characteristic changes in the physiological components of cybersickness,” *Psychophysiology*, 2005.

[16] B. C. Min, S. C. Chung, Y. K. Min, and K. Sakamoto, “Psychophysiological evaluation of simulator sickness evoked by a graphic simulator,” *Applied ergonomics*, vol. 35, no. 6, pp. 549–556, 2004.

[17] R. S. Kennedy, N. E. Lane, K. S. Berbaum, and M. G. Lilienthal, “Simulator Sickness Questionnaire: An Enhanced Method for Quantifying Simulator Sickness,” *The International Journal of Aviation Psychology*, vol. 3, no. 3, p. 203, 1993.

[18] F. Lotte, M. Congedo, A. Lécuyer, F. Lamarche, and B. Arnaldi, “A review of classification algorithms for EEG-based brain-computer interfaces.,” *Journal of neural engineering*, vol. 4, no. 2, Jun. 2007.

[19] M. Kaper, P. Meinicke, U. Grossekathoefer, T. Lingner, and H. Ritter, “BCI competition 2003-data set IIb: support vector machines for the P300 speller paradigm,” *Biomedical Engineering, IEEE Transactions on*, vol. 51, no. 6, pp. 1073-1076, Jun. 2004.

[20] G. Pfurtscheller, C. Neuper, D. Flotzinger, and M. Pregenzer, “EEG-based discrimination between imagination of right and left hand movement,” *Electroencephalography and Clinical Neurophysiology*, vol. 103, no. 6, pp. 642-651, Dec. 1997.

[21] S. Chiappa and S. Bengio, “HMM and IOHMM modeling of EEG rhythms for asynchronous BCI systems,” in *European Symposium on Artificial Neural Networks, ESANN*, 2004, pp. 193–204.

[22] J. del R. Millán and J. Mouriño, “Asynchronous BCI and local neural classifiers: an overview of the Adaptive Brain Interface project,” *IEEE Transactions on Neural Systems and Rehabilitation Engineering: A Publication of the IEEE Engineering in Medicine and Biology Society*, vol. 11, no. 2, pp. 159-161, Jun. 2003.

[23] W. D. Penny, S. J. Roberts, E. A. Curran, and M. J. Stokes, “EEG-based communication: a pattern recognition approach,” *Rehabilitation Engineering, IEEE Transactions on*, vol. 8, no. 2, pp. 214-215, Jun. 2000.

[24] G. Pfurtscheller, C. Neuper, A. Schlögl, and K. Lugger, “Separability of EEG signals recorded during right and left motor imagery using adaptive autoregressive parameters,” *IEEE Transactions on Rehabilitation Engineering: A Publication of the IEEE Engineering in Medicine and Biology Society*, vol. 6, no. 3, pp. 316-325, Sep. 1998.

[25] T. Wang, J. Deng, and B. He, “Classifying EEG-based motor imagery tasks by means of time-frequency synthesized spatial patterns,” *Clinical Neurophysiology: Official Journal of the International Federation of Clinical Neurophysiology*, vol. 115, no. 12, pp. 2744-2753, Dec. 2004.

[26] L. Qin, L. Ding, and B. He, “Motor Imagery Classification by Means of Source Analysis for Brain Computer Interface Applications,” *Journal of neural engineering*, vol. 2, no. 4, pp. 65-72, Dec. 2005.

[27] B. Kamousi, Z. Liu, and B. He, "Classification of motor imagery tasks for brain-computer interface applications by means of two equivalent dipoles analysis," *IEEE Transactions on Neural Systems and Rehabilitation Engineering: A Publication of the IEEE Engineering in Medicine and Biology Society*, vol. 13, no. 2, pp. 166-171, Jun. 2005.

[28] M. Congedo, F. Lotte, and A. Lécuyer, "Classification of movement intention by spatially filtered electromagnetic inverse solutions," *Physics in Medicine and Biology*, vol. 51, no. 8, pp. 1971-1989, 2006.

[29] P. Herman, G. Prasad, T. M. McGinnity, and D. Coyle, "Comparative Analysis of Spectral Approaches to Feature Extraction for EEG-Based Motor Imagery Classification," *IEEE Transactions on Neural Systems and Rehabilitation Engineering*, vol. 16, no. 4, pp. 317-326, 2008.

[30] D. Mantini, M. G. Perrucci, C. Del Gratta, G. L. Romani, and M. Corbetta, "Electrophysiological signatures of resting state networks in the human brain," *Proceedings of the National Academy of Sciences*, vol. 104, no. 32, pp. 13170 -13175, 2007.

[31] D. A. Peterson, J. N. Knight, M. J. Kirby, C. W. Anderson, and M. H. Thaut, "Feature selection and blind source separation in an EEG-based brain-computer interface," *EURASIP journal on applied signal processing*, vol. 2005, pp. 3128–3140, 2005.

[32] Y.-P. Lin, C.-H. Wang, T.-P. Jung, T.-L. Wu, S.-K. Jeng, J.-R. Duann, and J.-H. Chen, "EEG-based emotion recognition in music listening.," *IEEE Transactions on Biomedical Engineering*, vol. 57, no. 7, pp. 1798-1806, 2010.

[33] D. Garrett, D. A. Peterson, C. W. Anderson, and M. H. Thaut, "Comparison of linear, nonlinear, and feature selection methods for eeg signal classification," *IEEE Transactions on Neural Systems and Rehabilitation Engineering*, vol. 11, no. 2, pp. 141-144, 2003.

[34] C.-T. Lin, L.-W. Ko, I.-F. Chung, T.-Y. Huang, Y.-C. Chen, T.-P. Jung, and S.-F. Liang, "Adaptive EEG-Based Alertness Estimation System by Using ICA-Based Fuzzy Neural Networks," *IEEE Transactions on Circuits and Systems I: Regular Papers*, vol. 53, no. 11, pp. 2469-2476, 2006.

[35] C.-S. Wei, L.-W. Ko, S.-W. Chuang, T.-P. Jung, and C.-T. Lin, "EEG-based Evaluation System for Motion Sickness Estimation," *Proceedings of the 5th International IEEE EMBS Conference on Neural Engineering*, 2011.

[36] C.-S. Wei, L.-W. Ko, S.-W. Chuang, T.-P. Jung, and C.-T. Lin, "Genetic Feature Selection in EEG-Based Motion Sickness Estimation," presented at the International Joint Conference on Neural Networks (IJCNN 2011), San Jose, California, USA, 2011.

[37] I. Guyon and A. Elisseeff, "An introduction to variable and feature selection," *The Journal of Machine Learning Research*, vol. 3, pp. 1157–1182, Mar. 2003.

[38] B. Raman and T. R. Ioerger, "Enhancing Learning using Feature and Example Selection," *DEPARTMENT OF COMPUTER SCIENCE, TEXAS A&M UNIVERSITY*, 2003.

[39] D. E. Goldberg, *Genetic Algorithms in Search, Optimization, and Machine Learning*, 1st ed. Addison-Wesley Professional, 1989.

[40] D. Flotzinger, M. Pregenzer, and G. Pfurtscheller, "Feature selection with distinction sensitive learning vector quantisation and genetic algorithms," in *Neural Networks, 1994. IEEE World Congress on Computational Intelligence., 1994 IEEE International Conference on*, 1994, vol. 6, pp. 3448–3451.

[41] R. Oostenveld and T. F. Oostendorp, "Validating the boundary element method for forward and inverse EEG computations in the presence of a hole in the skull," *Human Brain Mapping*, vol. 17, no. 3, pp. 179-192, Nov. 2002.

[42] A. Delorme and S. Makeig, "EEGLAB: an open source toolbox for analysis of single-trial EEG dynamics including independent component analysis," *Journal of Neuroscience Methods*, vol. 134, no. 1, pp. 9-21, Mar. 2004.

[43] C.-T. Lin, C.-J. Chang, B.-S. Lin, S.-H. Hung, C.-F. Chao, and I.-J. Wang, "A Real-Time Wireless Brain-Computer Interface System for Drowsiness Detection," *Biomedical Circuits and Systems, IEEE Transactions on*, vol. 4, no. 4, pp. 214-222, Aug. 2010.

[44] C.-T. Lin, L.-W. Ko, J.-C. Chiou, J.-R. Duann, R.-S. Huang, S.-F. Liang, T.-W. Chiu, and T.-P. Jung, "Noninvasive Neural Prostheses Using Mobile and Wireless EEG," *Proceedings of the IEEE*, vol. 96, no. 7, pp. 1167-1183, 2008.

[45] J. Moody and C. J. Darken, "Fast learning in networks of locally-tuned processing units," *Neural Computation*, vol. 1, pp. 281–294, Jun. 1989.

[46] H. Drucker, C. J. C. Burges, L. Kaufman, A. Smola, and V. Vapnik, "Support Vector Regression Machines," *Advances in Neural Information Processing Systems*, vol. 9, pp. 155-161, 1996.

[47] H. Akaike, "A new look at the statistical model identification," *Automatic Control, IEEE Transactions on*, vol. 19, no. 6, pp. 716- 723, Dec. 1974.

[48] A. Subasi, "EEG signal classification using wavelet feature extraction and a mixture of expert model," *Expert Systems with Applications*, vol. 32, no. 4, pp. 1084-1093, May. 2007.

[49] Y. H. Yu, P. C. Lai, L. W. Ko, C. H. Chuang, B. C. Kuo, and C. T. Lin, "An EEG-based classification system of Passenger's motion sickness level by using feature extraction/selection technologies," *Proceedings of the 2010 International Joint Conference on Neural Networks (IJCNN)*, 2010.

[50] I. T. Jolliffe, *Principal Component Analysis*, 2nd ed. Springer, 2002.

[51] J. Fruitet, D. J. McFarland, and J. R. Wolpaw, "A comparison of regression techniques for a two-dimensional sensorimotor rhythm-based brain–computer interface," *Journal of Neural Engineering*, vol. 7, 2010.

[52] I. T. Jolliffe, "A Note on the Use of Principal Components in Regression," *Journal of the Royal Statistical Society. Series C (Applied Statistics)*, vol. 31, no. 3, pp. 300-303, Jan. 1982.